4 The Wave Energy Resource

Stephen Barstow, Gunnar Mørk

Fugro OCEANOR,
Trondheim, Norway

Denis Mollison

Heriot-Watt University,
Edinburgh, Scotland, UK

João Cruz

Garrad Hassan and Partners Ltd
Bristol, England, UK

On an average day, about 1 *TWh* of wave energy enters the coastal waters of the British Isles. It is tempting to call this amount huge - it is about the same as the total energy of the terrible Indian Ocean tsunami of the 26th of December 2004. It brings home the scale of human energy demands to realise that this is also about the same amount of energy which is used in electricity in the British Isles on an average day.

The same approximate equivalence holds at a world scale: the total wave energy resource is of the same order of magnitude as world electricity consumption ($\sim 2\ TW$). The exploitable limit is probably at most about 10–25 % of the resource; thus ocean wave energy is potentially a significant contributor to human energy demands, not a panacea. Its key advantages are that it comes in a high quality form - mechanical energy of oscillation - and that it travels very long distances with little loss, so that small inputs over a large ocean can accumulate and be harvested at or near the ocean's edge. Other advantages include the point absorber effect, whereby devices can extract energy from a fraction of a wavelength on either side; this makes small devices, with capacities of the order of 1 *MW*, relatively attractive.

4.1 The Resource and its Origin

Wave energy is created by wind, as a by-product of the atmosphere's redistribution of solar energy. The rate of energy input to waves is typically .01 to .1 W/m^2. This is a small fraction of the gross solar energy input, which averages 350 W/m^2,

but waves can build up over oceanic distances to energy densities averaging over 100 *kW/m* (note that the typical measure is power per metre width of wave front). Because of its origin from oceanic winds, the highest average levels of wave power are found on the lee side of temperate zone oceans.

Estimation of the resource is crucial when selecting suitable sites. In section 4.5.4 details on how available global wave model data, global satellite altimetry and measured buoy data were integrated in the EU supported WorldWaves project to derive a global wave and wind database with enhanced quality are given. Essentially, 10-years of 6 hourly wave and wind parameter data have been derived for 10,000 offshore grid points worldwide on a 0.5º grid. Based on these data sets, a number of global maps were produced. These are used in the following sections when discussing the global wave energy resource.

Firstly, Fig. 4.1 shows the 10-year mean annual wave power for all global points in the WorldWaves database. This map shows clearly that the most energy-rich areas of the global oceans are in the mid to high latitude temperate storm belts of both hemispheres, in particular between 40 and 60º. This figure gives, however, a slightly wrong impression of the relative energy levels in both hemispheres. The much higher resources in the southern hemisphere, where seasonal variations are much lower (compare Figures 4.2 and 4.3 showing January and July means), are seen more clearly in Fig. 4.4, where the mean wave power for all grid points is plotted as a function of latitude both annually and for the months of January and July.

On an annual basis, the highest levels in the Northern Hemisphere are off the west coast of the British Isles (see also Fig. 4.5) and Iceland and Greenland, with somewhat lower energy levels in the Pacific off the western seaboard of the US and Canada. Not surprisingly, the highest overall 50–100 *m* depth offshore energy levels in the Southern Hemisphere are located off Southern Chile, South Africa and the entire south and south west coasts of Australia and New Zealand. In equatorial waters, wave power levels of 15–20 *kW/m* on an annual basis over parts of all the ocean basins are observed, the highest coastal resources being off Northern Peru and Ecuador, although there may be significant El-Nino induced inter-annual variability in this area. Finally, in medium latitudes, Western Australia comes out best, with California also having a relatively high resource for the latitude.

Where in the world can the highest wave power regime be found? This turns out to be in the Southern Ocean at or around 48ºS, 90ºE which is about 1,400 *km* east of Kerguelen Island. Here, the annual average exceeds 140 *kW/m*. In the Northern Hemisphere, the maximum is found at 57ºN, 21ºW, some 400 *km* west of Rockall. Here, a "modest" by comparison 90 *kW/m* can be found. The maximum global monthly power level is practically the same in the two hemispheres, at or just above 200 *kW/m*. Note that these locations are given as example and are clearly unsuitable for wave energy projects: the mere distance to shore (and depth) is enough to make them unattractive. It is estimated that the first wave energy farms will be deployed in the 50–60 *m* depth region, i.e., in the limit of the transition from nearshore to the more attractive offshore wave climates.

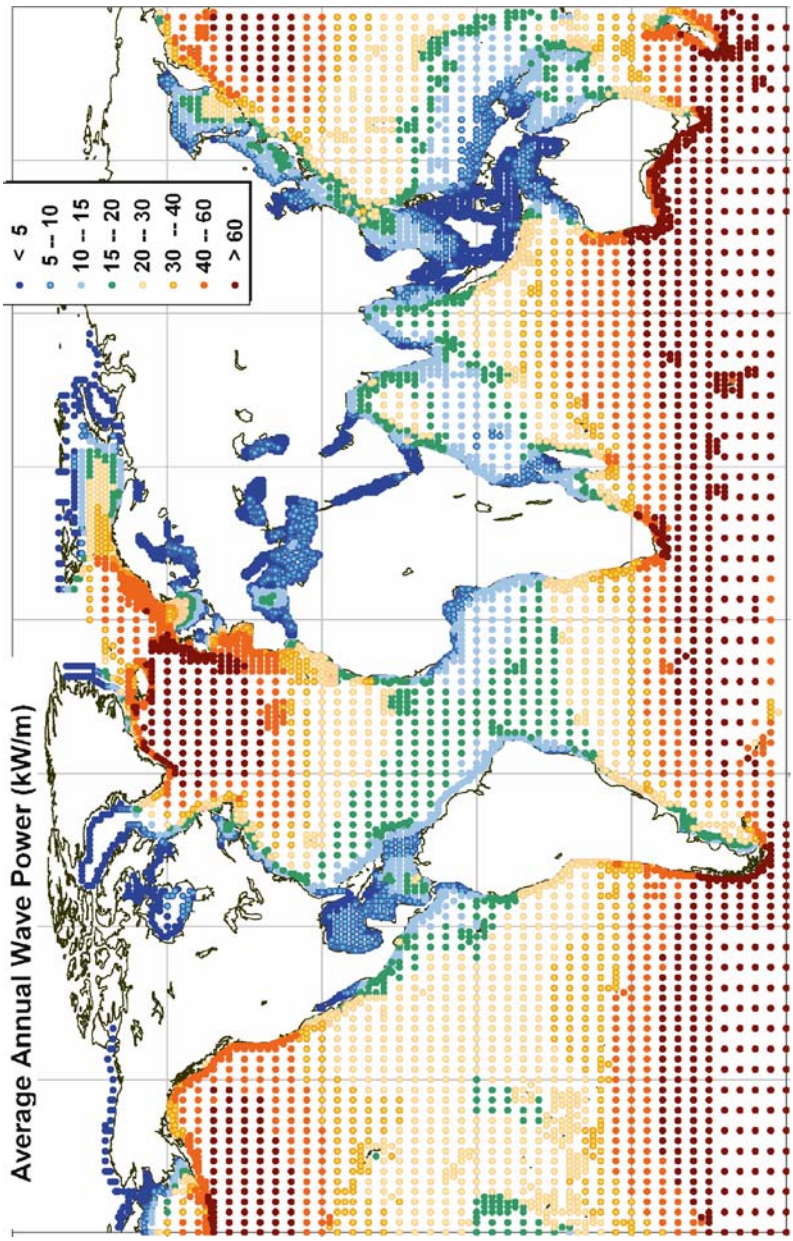

Fig. 4.1. Global annual mean wave power estimates in kW/m (data from the ECMWF WAM model archive; calibrated and corrected by Fugro OCEANOR against a global buoy and Topex satellite altimeter database)

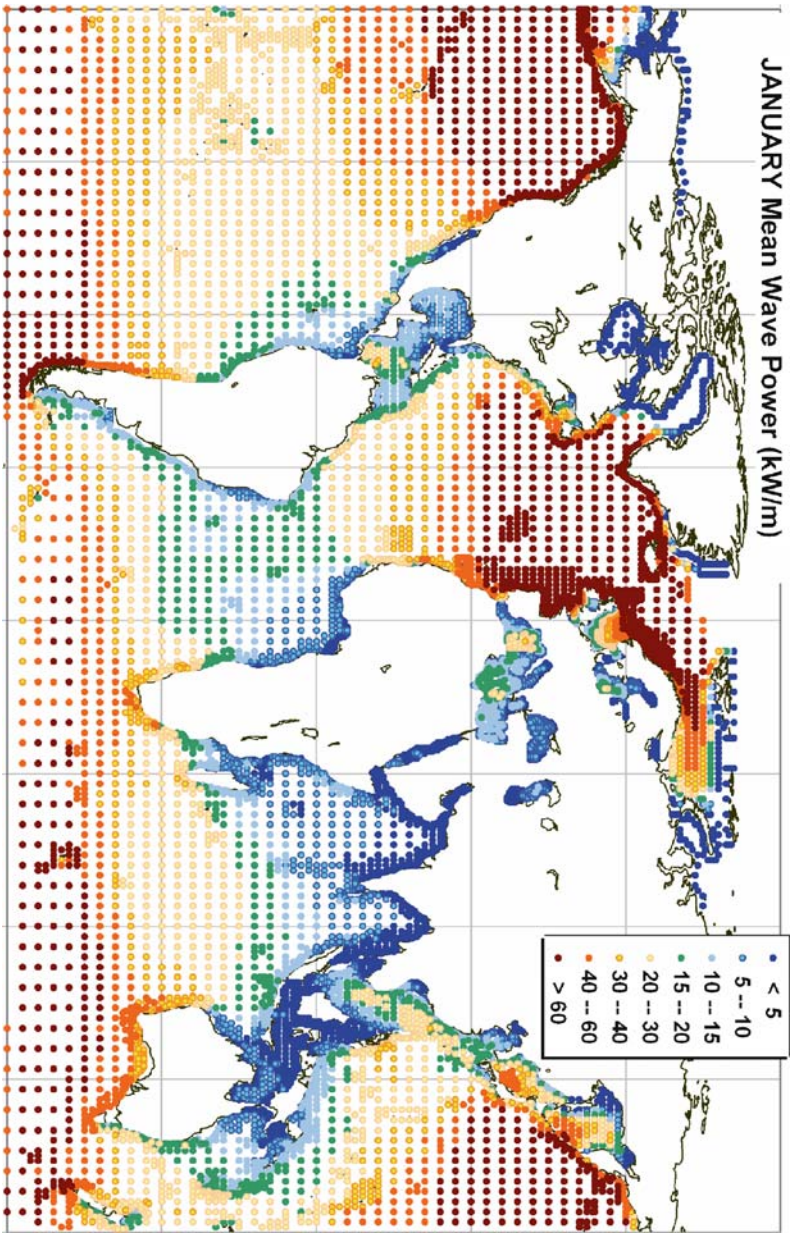

Fig. 4.2. Global January mean wave power estimates in kW/m (data from the ECMWF WAM model archive; calibrated and corrected by Fugro OCEANOR against a global buoy and Topex satellite altimeter database)

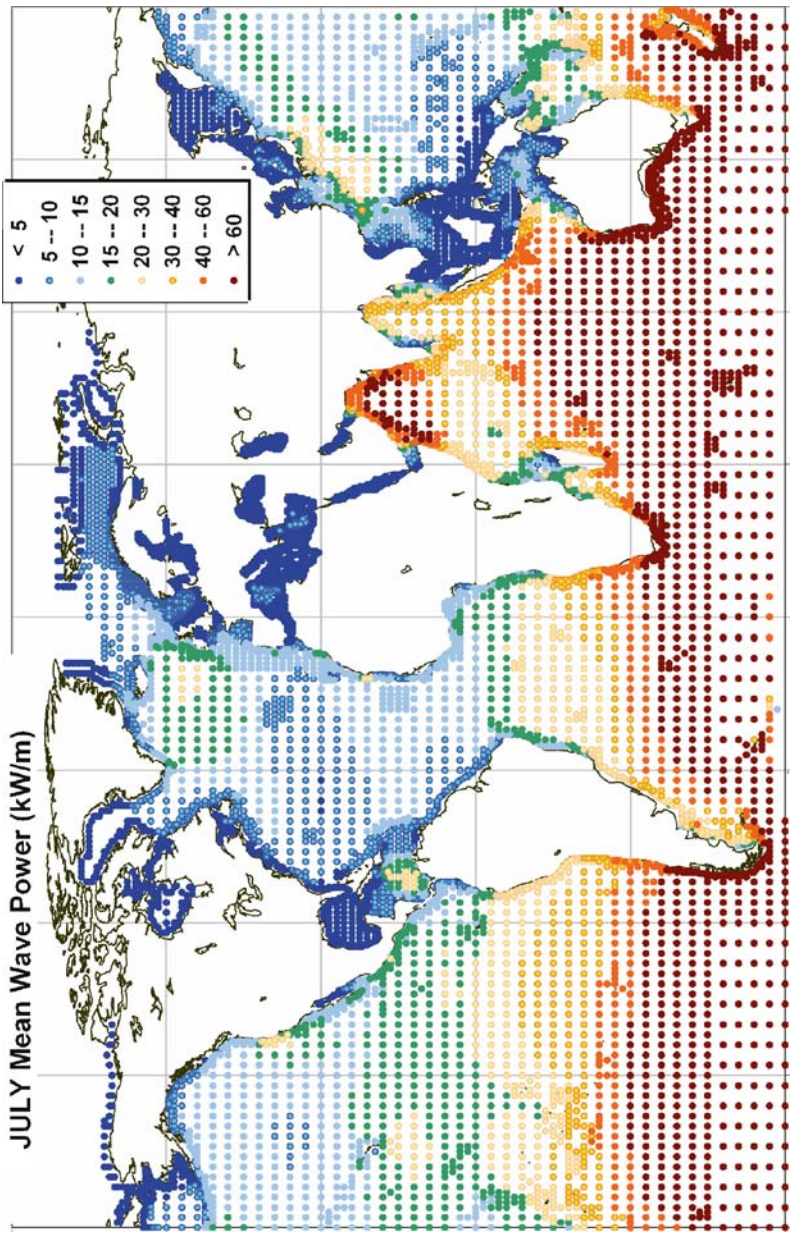

Fig. 4.3. Global July mean wave power estimates in kW/m (data from the ECMWF WAM model archive; calibrated and corrected by Fugro OCEANOR against a global buoy and Topex satellite altimeter database)

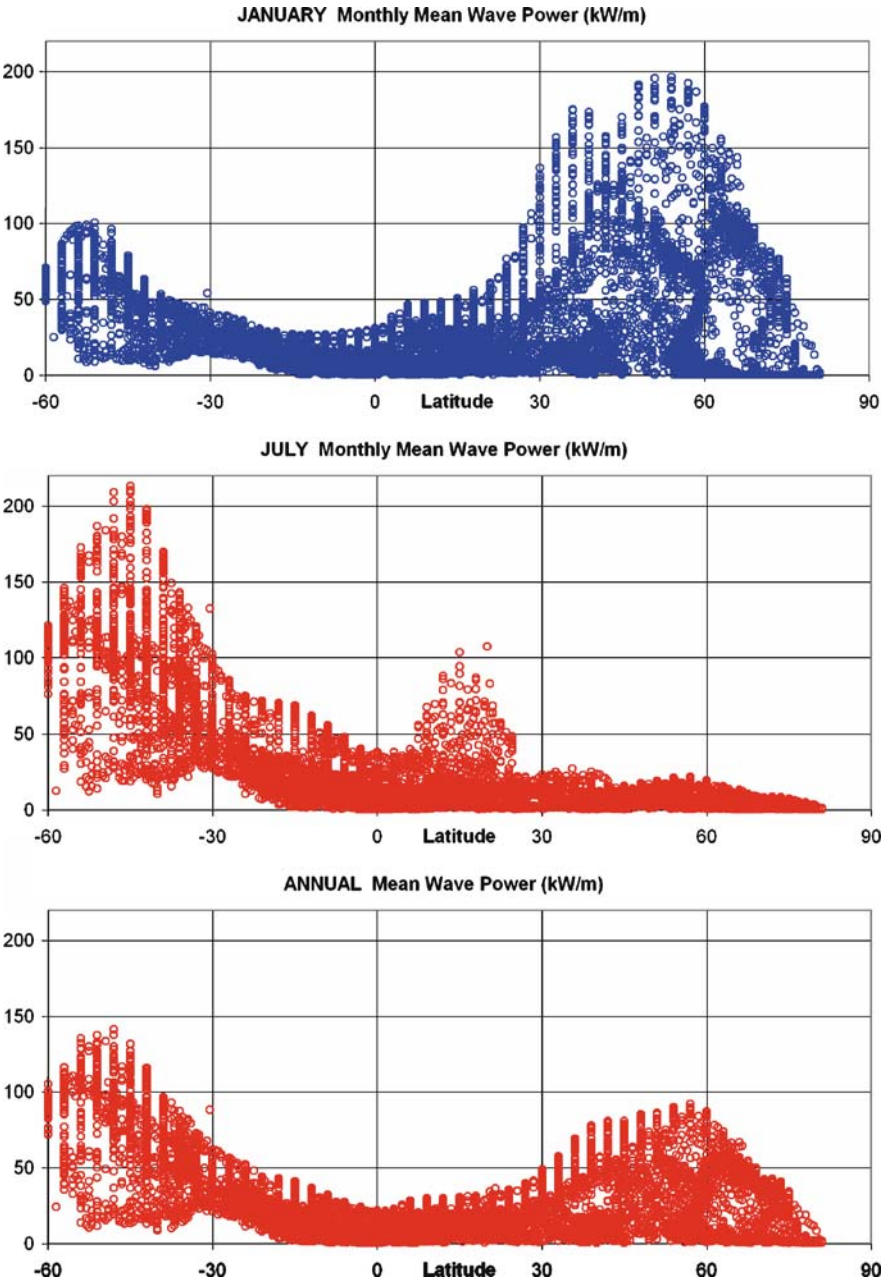

Fig. 4.4. Variation in mean monthly and (bottom) annual wave power against the latitude for all global grid points

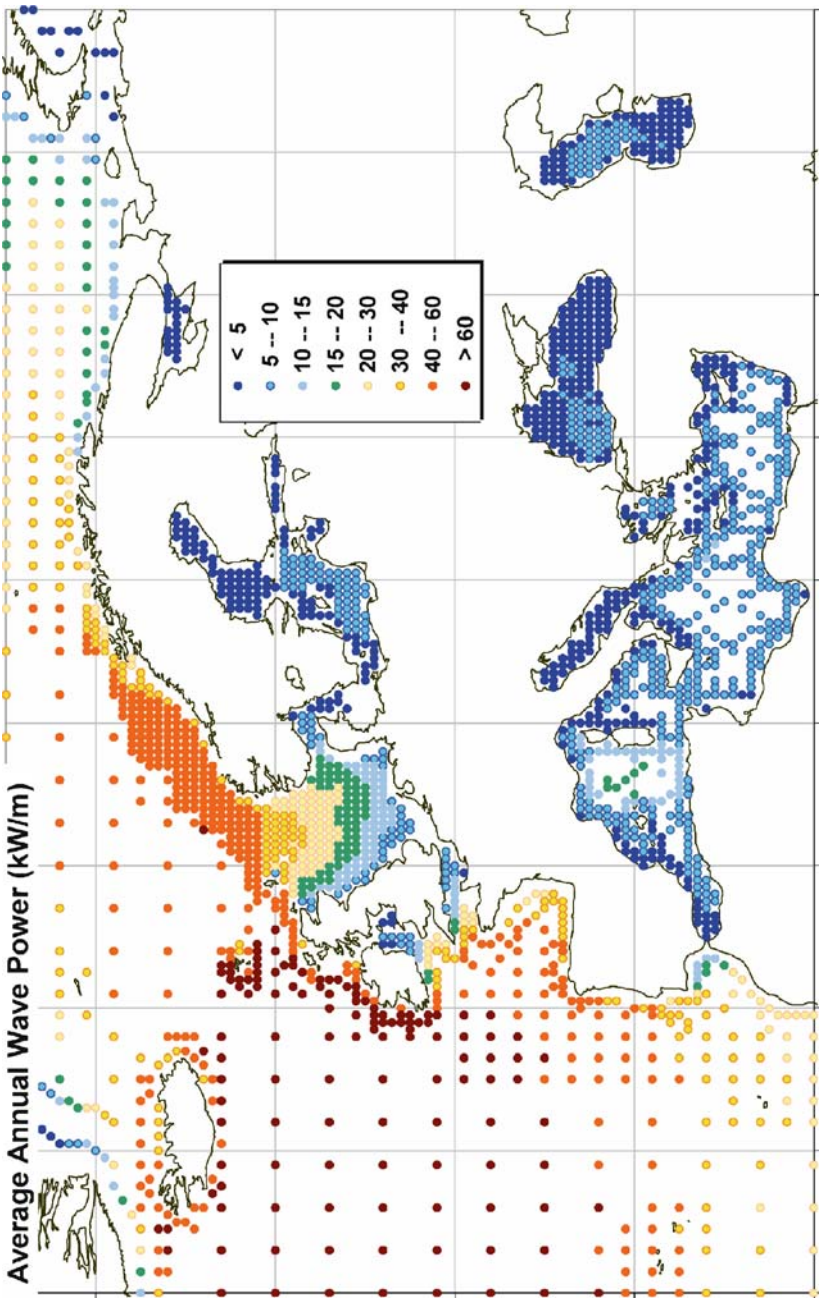

Fig. 4.5. Annual mean wave power estimates (*kW/m*) for European waters (data from the ECMWF WAM model archive; calibrated and corrected by Fugro OCEANOR against a global buoy and Topex satellite altimeter database)

Figures 4.2 and 4.3 give an indication of the seasonality of the global resources. However, if the ratio of the minimum monthly power level against the annual mean is evaluated, a clearer idea of how the resource varies over the year is obtained (Fig. 4.6). Figure 4.7 presents this data in a different way showing the variation of the same statistic against latitude. There is a dramatic difference between hemispheres as far as the stability of the wave energy resources is concerned with large summer to winter changes in the north, the largest being in ice impacted waters.

There are also large seasonal changes in the monsoon areas of South East Asia due to the seasonal switch in wind direction in these areas. This is particularly large along seasonally downwind and upwind coastlines, or indeed two sides of an oceanic island, due to the influence of fetch on wind wave growth. In the South China Sea, the seasonality is large due to the fact that there is little swell to smooth out the seasonal wind sea changes. This is also a dominant feature of the Arabian Sea which, along, with the Bay of Bengal, are the only sea areas in the Northern Hemisphere with larger summer than winter energy levels, due to a combination of stronger summer monsoon winds and higher swell influx at that time of year (i.e., the Southern Ocean winter). Another interesting feature is the area of the southern Indian Ocean to the south and west of Australia which shows regionally surprisingly large seasonality. This is due to the fact that this area roughly corresponds to the location, in January, of the Indian Ocean Anticyclone. This anticyclone has a remarkably large seasonal displacement towards the west during winter, leading to a large seasonal change in storm frequency in the aforementioned area.

In coastal areas, it can be seen that there are particularly stable wave energy resources off Chile, Namibia, Eastern Australia, Sierra Leone and Liberia, the Pacific coasts of Mexico and most of the South Pacific island nations, although these nations, particularly the low lying ones, are nowadays concerned with wave power for other reasons.

Finally, Fig. 4.8 plots the relationship between the extreme and mean significant wave height. One can consider, in very simple terms, that the lower this ratio is, the more feasible a wave energy project might be as the extreme conditions relate to design and to a certain extent operational costs and the mean represents the resource or the income (see also Hagerman, 1985, who introduced a similar ratio, his Figure of Merit). The change in this ratio from deep water to shallow water is particularly interesting, and is discussed further in section 4.5.

In terms of resource, there are many attractive areas in the globe when looking for a suitable site to locate a wave energy farm, as Figs. 4.1 to 4.8 suggest. The challenge is to choose a location which provides not only the adequate resource but also all the necessary conditions to ensure the continuous and reliable operation of the wave energy converters. A key driver is the proximity to shore, linked also with the water depth, as it influences not only costs (e.g. underwater power cables) but mostly the possibility of safely recovering the devices and conducting maintenance in a local shipyard. All of these variables (resource, cost, O&M) need to be carefully measured and given considerable thought.

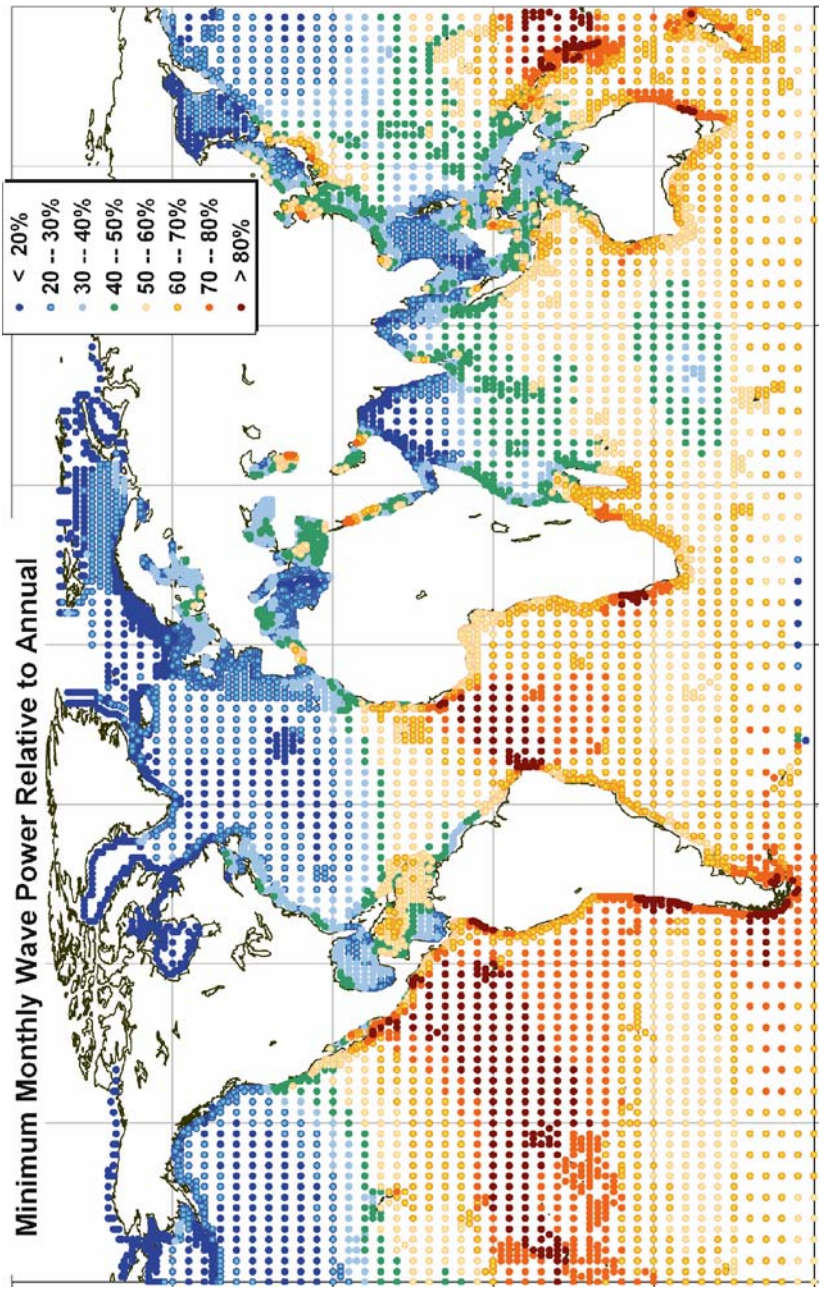

Fig. 4.6. The ratio of the minimum of the individual monthly wave power estimates to the annual value gives an indication of the seasonal variability of the resource (data from the ECMWF WAM model archive; calibrated and corrected by Fugro OCEANOR against a global buoy and Topex satellite altimeter database)

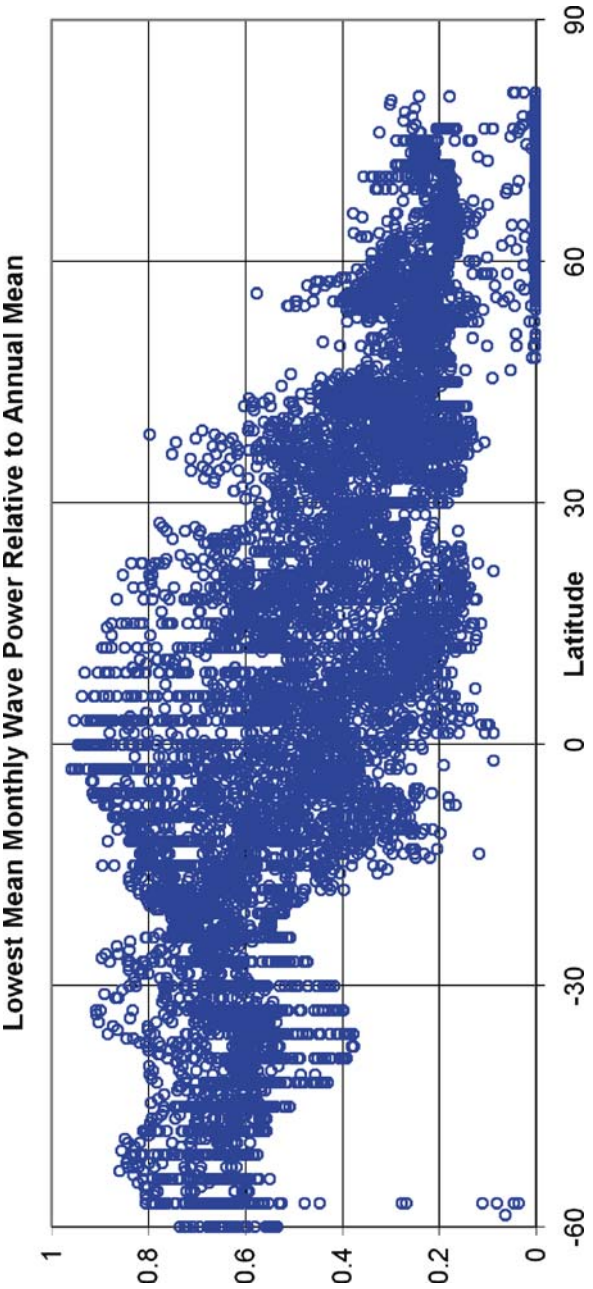

Fig. 4.7. Variation in the ratio of the minimum of the individual monthly wave power estimates to the annual value against latitude shows clearly the much lower seasonality in the far south. Note that the grid points with zero are from areas impacted by ice in the northern hemisphere

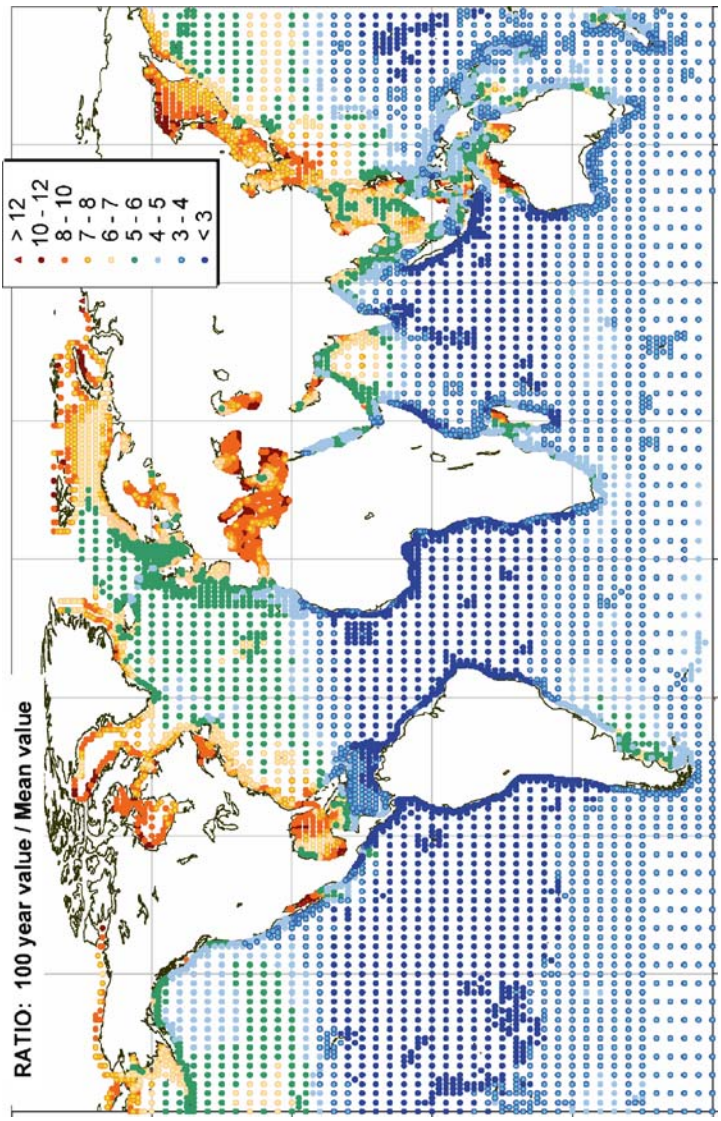

Fig. 4.8. The ratio of the 100-year significant wave height to the mean wave height, inspired by Hagerman's Figure of Merit (1985), roughly reflects the ratio of design costs for a wave energy plant against its income (the resource). The lower this ratio, the better it is. The 100-year value is calculated by a simple extrapolation of the 10-year significant wave height distribution at each location fitted by a 3-parameter Weibull distribution. Note that this ratio may be underestimated in areas impacted by hurricanes, cyclones, typhoons and other extreme events with long return period as 10-years is then not sufficiently long for reliable extreme estimates using this method (data from the ECMWF WAM model archive; calibrated and corrected by Fugro OCEANOR against a global buoy and Topex satellite altimeter database)

4.2 Sea States and their Energy

Deep water surface waves are oscillations of the sea surface layer under gravity and, to a good approximation, they consist of the linear superposition of a large number of simple components. This basic component is a sinusoidal wavetrain, with period T, which appears to travel at its phase velocity, $U = gT/2\pi$.

In fact, the water particles are not travelling: in a simple sinusoidal wave they oscillate in circles, whose amplitude a_d falls off exponentially with depth d ($a_d = a \exp(-2\pi /L)$).

The energy of the wavetrain, per unit area, is $E = \rho g H^2$, where ρ is the density of the water and H the root mean square wave height ($H^2 = a^2/2$). More crucially for the present purposes, the oscillations move energy in the direction of the wavetrain and this energy flux, i.e. power per unit width, is E multiplied by the group velocity $U/2$, resulting in cH^2T, where the constant c is given by $\rho g^2/4\pi$ ($\cong 7.87\, kW/m^3s$).

Following the linear superposition assumption, a general sea state can therefore be described by its directional spectral density, $S(f,\theta)$, which specifies how the energy is distributed over frequencies (f) and directions (θ). Note that to specify the instantaneous sea state the phase is also required.

The power in a general sea state is the integral of the energy density multiplied by the group velocity. The spectral moments (m_n) are particularly useful to quantify the power; m_n denotes the nth moment of the frequency spectrum, given by

$$m_n = \int f^n S(f) df \,. \tag{4.1}$$

A selection of spectral parameters is typically used to characterise a sea state. In an effort to standardise the nomenclature the spectral approach is used throughout this chapter. But firstly some short notes on alternative nomenclatures / definitions are presented. To understand the original definitions it is necessary to recall a typical plot of a wave record (surface elevation vs. time). In a pre-computational environment to process such a plot meant subtracting the mean water level and searching for the point where the surface profile crosses the zero line upwards. Such a point identifies the start of a new wave. The next zero-upcrossing point would then define the end of this wave and the start of the next one (Goda, 2000). Extreme individual values could be easily extracted, such as the maximum wave height (H_{max}) and maximum wave period (T_{max}) in a record, but once the waves are identified and counted, other parameters could also be derived. In terms of wave height, the mean wave, the highest one-tenth ($H_{1/10}$) and the highest one-third ($H_{1/3}$) wave are the most interesting from a statistical point of view.

The significant wave height (H_s), a standard measure in the offshore industry, is by definition $H_{1/3}$: the waves in a record were counted and selected, in descending order starting from the highest wave until one-third of the total number of waves was reached. The mean value is $H_{1/3}$. The same procedure could be applied to the wave period, resulting in $T_{1/3}$, the significant wave period.

When trying to link Eq. (4.1) to H_s, it was found that $H_{1/3}$ is approximately $4\sqrt{m_0}$, which therefore corresponds to the significant wave height when using a spectral approach (H_{m0}). Note that the relation between H_{m0} and the root mean square wave height (H_{rms}) is also clear ($H_{m0} = 4H_{rms}$), which could suggest that the use of H_{rms} is particularly suitable to keep the physical meaning (but it is particularly unsuited when comparing it to the standard significant wave height). Overall the spectral approach is mathematically consistent, as Table 4.1 suggests. Every parameter can thus be obtained from Eq. (4.1). Knowing the relation between H_{m0} and H_{rms}, the wave energy flux can be therefore given by $\frac{c}{16}H_{m0}^2 T_{-10}$, in *W/m*, for deep water waves ($c = \rho g^2/4\pi, \cong 7.87\, kW/m^3 s.$).

To estimate the directional content of a given sea state is also of vital importance to both the characterisation of a specific site and to predict the performance of a wave energy converter. In order to fully define the directional spectra $S(f,\theta)$ several methods can be applied.

Two basic approaches are possible, following either stochastic or deterministic methods. The methods have specific limitations and potential, and differ considerably in terms of the degree of parameterisation and on the computational effort required, for the same frequency and directional resolution. An overview of the main methods is given is subsections 4.2.1 and 4.2.2, following Benoit et al. (1997).

Stochastic methods are based on the random phase assumption. The cross-spectrum between each pair of signals is calculated, and the directional spectrum is derived by inverting the relation with the cross-spectra, using one of the available techniques. The form of the directional spreading function, which if convoluted with the frequency spectrum results in the directional spectrum, is always assumed, but major differences exist when fitting the data to the model: Fourier expansions use a deterministic fit, parametrical models use fixed form functions and the latest generation of methods, like the Maximum Likelihood Method (MLM) or Maximum Entropy Method (MEM), fit statistically to the data. The latter class is by far the best option when modelling real data following a stochastic approach, particularly when evaluating data from directional wave buoys or any other single-point system.

Table 4.1. Definition of the key spectral parameters

Spectral Nomenclature	Definition	Description
H_{m0}	$4\sqrt{m_0}$	Significant wave height (H_s)
T_{-10}	m_{-1}/m_0	Energy period (T_e)
T_{02}	$\sqrt{m_0/m_2}$	Zero-upcrossing period (T_z)

Deterministic methods keep the phase information but only allow one or two directions per frequency. The cross-spectrum is not evaluated and the Fourier coefficients from each individual signal are used. The number of methods is much smaller than the stochastic equivalents and only two are typically used. The approach might prove useful in cases where reflective structures are present.

4.2.1 Directional Spectra Estimation Using Stochastic Methods

In the stochastic approach it is assumed that the wave field can be described by

$$\eta(x,y,t) = \iint \sqrt{2S(f,\theta)\,df d\theta}\cos\left[k\left(x\cos\theta + y\sin\theta\right) - 2\pi ft + \varphi\right], \quad (4.2)$$

where $\eta(x,y,t)$ is the surface elevation, $S(f,\theta)$ the directional spectrum, k the wave number, θ the wave direction, f the wave frequency and φ the phase function. Stochastic methods carry the assumption that φ is randomly disturbed over the entire $[0,2\pi]$ range with uniform probability density, which in turn means that all wave components are treated as independent of each other. When analysing situations where phase-locked waves are present (e.g.: in the vicinity of a reflective formation) such assumption might be biased. All these methods follow a two step approach:

1. Computation of the cross-spectra between each pair of signals, usually by means of the Fast Fourier Transform;
2. Calculation of the directional spreading function, using the relation between the cross-spectra and the directional spectra and one of the methods below described.

The relation mentioned in 2. can be given by

$$G_{ij}(f) = E(f)\int_0^{2\pi} H_i(f,\theta)H_j^*(f,\theta)e^{-i\vec{k}\cdot\left(\vec{x}_j-\vec{x}_i\right)}D(f,\theta)\,d\theta, \quad (4.3)$$

where $G_{ij}(f)$ is the cross-spectra, $E(f)$ the frequency spectra derived from the surface elevation signal, $H_m(f,\theta)$ the transfer function between the surface elevation and another wave signal (e.g.: pressure, horizontal velocity, etc.)[1], and $D(f,\theta)$ the directional spreading function.

To solve the system of equations that Eq. (4.3) represents, the first step is to calculate the cross-spectra of the original signals[2]. The output can be rearranged in

[1] '*' denotes the complex conjugate.

[2] Given the complex nature of the cross-spectra, the real part is typically called coincident or co-spectrum and imaginary one quadrature or quad-spectrum.

terms of Fourier Coefficients. For single point measurement systems with three independent signals (e.g: Waverider buoy, ADCP), only four coefficients can be calculated, irrespective of the method followed to calculate $D(f,\theta)$. These methods differ considerably in several assumptions and computing potential, and will therefore lead to different results. $D(f,\theta)$ has some inherent proprieties, namely

$$\int_0^{2\pi} D(f,\theta)d\theta = 1, \tag{4.4}$$

which follows from $E(f) = \int_0^{2\pi} S(f,\theta)d\theta$. In addition: $D(f,0) = D(f,2\pi)$ and the spreading function is also positive over the $[0,2\pi]$ interval, a condition that some less precise methods fail to obey, producing erroneous results.

There is a vast amount of stochastic methods available for calculating $D(f,\theta)$ in order to solve Eq. (4.3). Some of them can be grouped in classes like Fourier Series Decomposition or Parametrical methods.

For the first class, which can be understood as an introduction, two different methods were reviewed.

Truncated Fourier Series Decomposition Method (TFSM)

The Fourier series expansion of $D(f,\theta)$ is given by

$$D(f,\theta) = \frac{a_0}{2\pi} + \frac{1}{\pi}\sum_{n=1}^{\infty} a_n \cos n\theta + b_n \sin n\theta, \tag{4.5}$$

with

$$a_0 = \int_0^{2\pi} D(f,\theta)d\theta = 1. \tag{4.6}$$

In the simplest form, the series is reduced to a finite number of terms (*N*). If $N=2$ (single point measuring systems) only (a_1,b_1) and (a_2,b_2) are calculated from Eq. (4) it is possible to obtain

$$D(f,\theta) = \frac{1}{\pi}\left(\frac{1}{2} + a_1\cos\theta + b_1\sin\theta + a_2\cos 2\theta + b_2\sin 2\theta\right). \tag{4.7}$$

Although computationally efficient, the method yields the serious drawback of outputting negative values for the directional spreading function in some occasions, which is inherently flawed (Kuik et al., 1988). Refinements of this method include a weighting function that will ensure that an everywhere positive $D(f,\theta)$ (e.g.: Longuet-Hinggins et al., 1963). Note that Eqs. (4.5) and (4.7) have a deter-

ministic nature but the methods are intrinsically stochastic, given the random phase assumption.

Direct Fourier Transform Method (DFTM)

A refinement of the TFS method is available in Kinsman (1963), following earlier work from Barber (1961). Again a Fourier expansion is made, but of greater complexity, resulting in

$$D(f,\theta) = \alpha\left\{1 + 2\sum_{n=1}^{j}\left[C_{ij}^{'}\cos\left(kX_n\cos\theta + kY_n\sin\theta\right) + \right.\right. \\ \left.\left. + Q_{ij}^{'}\sin\left(kX_n\cos\theta + kY_n\sin\theta\right)\right]\right\}, \tag{4.8}$$

where $C_{ij}^{'}$ and $Q_{ij}^{'}$ are the normalised components of the co and quad-spectra, respectively, and X_n and Y_n the spatial lags linked with the covariance function (recall that the cross-spectrum is the Fourier transform of the covariance function). α is a constant factor used to allow the unit integral condition over $[0,2\pi]$. The TFS and DFT methods produce similar (but not equal) results which are usually of lower quality when compared with methods which statistically fit to the data when solving the system of equations given by Eq. (4.3).

In conclusion, Fourier Series decomposition methods will lead to directional spectra estimations which typically have low spatial resolution. More recent approaches allow more accurate estimates, but it is still interesting to compare some parameters, like the mean direction, derived from all methods.

Parametrical methods use fitting techniques, either deterministic or statistically based, to derive $D(f,\theta)$. The common trend among them is the direct assumption (*a priori*) of a given shape for the directional energy distribution (Kuik et al., 1988). The models can also be unimodal or bimodal, where a linear combination of unimodal models is used. Cosine spreading functions are typically implemented (e.g: Mitsuyasu et al. 1975).

To avoid the Fourier decomposition and statistically fit the model to the data, Isobe (1990) initially developed a Maximum Likelihood Fitting method (MLF) that aimed to maximise a likelihood function linked with the Fourier coefficients of the signals. Some limitations, like the inability to detect two peaks at the same frequency, and mostly the availability of more efficient techniques lead directly to alternatives, neglecting this class of methods.

The evolution of the estimation techniques can be clearly predicted by looking at the first two classes of methods: to overcome the initial limitations that contribute to the rough estimates and sometime negative distributions the parametrical methods were derived. Although many shapes can be assumed, the number of available Fourier coefficients limits the number of shape parameters, which is a major weakness of the approach. Sand (1984) suggested a deterministic approach that would be further studied by Schäffer and Hyllested (1994), but a review on

some of the newer generation stochastic methods, like the Maximum Likelihood and Maximum Entropy methods, is firstly conducted.

Extended Maximum Likelihood Method (EMLM)

Following on the early work of Capon et al. (1967), the Maximum Likelihood method takes a linear combination of the cross-spectra,

$$D'(f,\theta)=\frac{1}{E(f)}\sum_{i,j}\alpha_{ij}(f,\theta)G_{ij}(f), \tag{4.9}$$

with

$$D'(f,\theta)=\int_0^{2\pi}D(f,\theta)w(\theta,\theta')d\theta'. \tag{4.10}$$

The EMLM spreading function estimate can then be considered as the convolution product of the true $D(f,\theta)$ with the window function $w(\theta,\theta')$. Naturally, the estimate and the real $D(f,\theta)$ will be more and more similar as $w(\theta,\theta')\to\delta(\theta,\theta')$, where $\delta(\theta,\theta')$ is the Dirac function. The window function is given by

$$w(\theta,\theta')=\sum_{i,j}\alpha_{ij}(f,\theta)H_i(f,\theta')H_j^*(f,\theta'). \tag{4.11}$$

Isobe et al. (1984) proved that the best $D'(f,\theta)$ is

$$D'(f,\theta)=\frac{\kappa}{\sum_{i,j}H_i(f,\theta)G_{ij}^{-1}(f)H_j^*(f,\theta)}, \tag{4.12}$$

where κ satisfies the unit integral condition over $[0,2\pi]$. One possible limitation associated with the method was pointed by Benoit and Teisson (1994) when testing numerical and laboratorial data, and is associated with its tendency to produce broader directional peaks. However such tendency is harder to quantify when real sea data is being used.

Iterated Maximum Likelihood Method (IMLM)

An alternative procedure to derive the MLM estimate was introduced by Pawka (1983), in an attempt to match the cross-spectra from the initial MLM estimate with the one from the original signals. This is directly linked with the influence of $w(\theta,\theta')$, as Eqs. (4.10) and (4.11) demonstrate, and follows from Eq. (4.12).

In the iterated version of the method a quantity $\varepsilon^i(f,\theta)$ is added to the derived spreading function in the previous iteration. $\varepsilon^i(f,\theta)$ can be given by

$$\varepsilon^i(f,\theta)=\frac{|\lambda|^{\beta+1}}{\lambda\gamma}, \tag{4.13}$$

with

$$\lambda = D'(f,\theta)-\Delta_{MLM}^{i-1}(f,\theta), \tag{4.14}$$

where $\Delta_{MLM}^{i-1}(f,\theta)$ stands for the MLM estimate computed from the cross-spectra based on $D'(f,\theta)$ (and not the original one). β and γ are control parameters that support the convergence of the iterative algorithm (as a rough guide, the order of magnitude of β and γ is 1 and 10, respectively). The iterative process is halted after a fixed number of iterations.

In Benoit et al. (1997) it is mentioned that the IMLM should produce a more precise estimate than the EMLM for single-point measurement systems. The tendency for producing more narrow banded spectra was confirmed when using data from Waverider buoys (see 4.2.3).

Extended Maximum Entropy Principle (EMEP)

Hashimoto et al. (1994) have extended the Maximum Entropy Principle (MEP) for arrays of measuring devices, with both by the original MEP and the EMEP producing identical results for single-point measuring systems such as a directional wave buoy. The EMEP algorithm follows:

$$D'(f,\theta)=\frac{1}{c}e^{\sum_{n=1}^{N}a_n\cos n\theta+b_n\sin n\theta}, \tag{4.15}$$

where $c=\int_0^{2\pi}e^{\sum_{n=1}^{N}a_n\cos n\theta+b_n\sin n\theta}d\theta$. The coefficients a_n and b_n are unknown and there is a total of M equations that can be used to solve the problem, with M being the non-zero components of the cross-spectra. Each equation can be written to illustrate the difference between the measured and the model cross-spectra, obtained by direct introduction of Eq. (4.15) in Eq. (4.3). This difference, as for the MLM, is not necessarily null, so a total of M residuals (ε_m, $m=1,...,M$) will appear. The optimal estimate is the one which minimises the sum of the squares of the residuals, a non-linear problem that can be solved using Newton's method. The optimal number of coefficients (N) is obtained by minimising the Akaike Information Criteria (AIC; Akaike, 1973):

$$AIC = M\left(\ln 2\pi+1+\ln\sigma^2+4N+2\right), \tag{4.16}$$

where σ^2 is the estimated variance of ε_m. The EMEP is therefore a powerful stochastic method, as the number of harmonic components given by Eq. (4.15) is

adapted to the data. In addition, statistical variability is also taken into account. Hashimoto et al. (1994) proved that the MEP and EMEP methods yield similar outputs for single-point measuring systems and in the process also reported the similarities with the outputs of the much more computationally intensive Bayesian Directional Method.

Bayesian Directional Method (BDM)

The Bayesian Directional Method (BDM) is the only stochastic method which does not assume any shape with regard to the directional spreading function. Such nature ensures that the method is highly adaptive, a desirable characteristic, but it also contributes to a difficult numerical implementation and a partly unsuitability for single-point measuring systems, as the computational time required is very high when compared to the conventional alternatives and the increase in accuracy is often minimum. Nevertheless, it is able to detect a broad variety of directional spectra, like uni, bi and trimodal, symmetrical peaks, etc.

The method was adapted from Bayesian techniques used in probability theory by Hashimoto et al. (1987). The $[0,2\pi]$ range is sub-divided into N segments, and the BDM estimate is a piecewise-constant function over each of the N segments. It is defined recursively as:

$$\begin{cases} x_n = \ln D'(f,\theta_n) \\ D'(f,\theta_n) = \sum_{n=1}^{N} e^{x_n} I_n(\theta) \end{cases}, \tag{4.17}$$

where

$$\begin{cases} \theta_n = (n-1/2)\Delta\theta = (2n-1)\pi/N \\ I_n(\theta) = \begin{cases} 1, & \text{if } (n-1)\Delta\theta \le \theta \le n\Delta\theta \\ 0, & \text{otherwise} \end{cases} \end{cases}. \tag{4.18}$$

The high value of N (typically between 40 and 90) and the statistical treatment that the errors in the estimated cross-spectra suffer lead to a very complete (and computationally intensive) approach. To add to the complexity, the non-linear system of equations is closed by a smoothness condition applied to the estimated directional spreading function:

$$\sum_{n=1}^{N} (x_{n+1} - 2x_n + x_{n-1})^2 \to 0, \tag{4.19}$$

with a parameter (or hyperparameter) linking the Eq. (4.19) and the system of equations given by the introduction of Eq. (4.17) in Eq. (4.3). This parameter corresponds to the one which minimises the Akaike Bayesian Information Criteria (ABIC; Akaike, 1973).

4.2.2 Directional Spectra Estimation Using Deterministic Methods

Deterministic methods have one very distinctive factor from stochastic approaches: the phase information is retained from the original data set, and not assumed to be randomly disturbed over the entire $[0,2\pi]$ range with uniform probability density. Furthermore, the cross-spectrum is not evaluated and the Fourier coefficients from each individual signal are used. The wave field is decomposed into wave components of a given direction, amplitude and phase (deterministic decomposition), and so the free surface elevation follows:

$$\eta(x,y,t)=\sum_{m=1}^{M}\sum_{n=1}^{N}a_{mn}\cos\left[k_m\left(x\cos\theta_n+y\sin\theta_n\right)-\omega_n t+\varphi_{mn}\right], \tag{4.20}$$

where *m* and *n* denote the frequency and directional bins, respectively. Deterministic methods assume a high value for *M* but a low value for *N* (i.e: $N=1$ or $N=2$), to ensure that the amplitude and the phase of the original signals can be determined from the Fourier coefficients. Such characteristic intrinsically limits the ability of the methods to model a wide range of directional spectra shapes, in a similar way to what occurs with parametric methods (in common they have the high level of parameterisation).

Deterministic methods are far scarcer than stochastic methods. Sand (1984) presents a review on the basic principles and Schäffer and Hyllested (1994) provide the two approaches that are commonly used: SDD and DDD, single and double directional decomposition, respectively.

Single Direction Decomposition (SDD)

The inputs for the SDD and DDD approaches are the same: the surface elevation and two horizontal velocities, (u,v). The Fourier transform of each signal is derived, resulting in C_η, C_u/F and C_v/F, respectively. F is the transfer function between the surface elevation and the horizontal velocity signals at a certain depth, as given by linear wave theory.

The SDD method has one main assumption: a three-dimensional sea can be represented by a sum of components of different frequencies. It is straightforward to implement this by considering the vector $\vec{u}_f(t)$, with

$$\begin{cases} u_f=\Re\left\{C_u e^{i\omega t}\right\} \\ u_v=\Re\left\{C_v e^{i\omega t}\right\} \end{cases}, \tag{4.21}$$

where $\Re$ denotes the real part, ω is the angular frequency and t is time. The norm of $\vec{u}_f(t)$ has two maxima and two minima, which appear for

$$\tan 2\omega t=\frac{2\left(A_u B_u+A_v B_v\right)}{A_u^2-B_u^2+A_v^2-B_v^2}, \tag{4.22}$$

where the A and B coefficients are given from $C_u = A_u - iB_u$ and $C_v = A_v - iB_v$. Considering that the two solutions which give the maxima are ωt and $\omega t + \pi$, the correct direction of propagation is chosen from the two by evaluating which leads to a positive η_f, with

$$\eta_f(t) = \Re\left\{C_\eta e^{i\omega t}\right\}. \tag{4.23}$$

Note that the amplitude and phase of the wave are linked with C_η, so the velocities are used only for deriving the wave direction from Eq. (4.22).

Double Direction Decomposition (DDD)

The DDD method assumes that two components (directions) exist per frequency. Such assumption allows it to be more suitable for situations where reflections are relevant. Knowing that the subscripts 1 and 2 refer the wave directions, the following decomposition can be obtained:

$$\begin{cases} C_\eta = C_{\eta_1} + C_{\eta_2} \\ C_u = C_{\eta_1}\cos\theta_1 + C_{\eta_2}\cos\theta_2 \\ C_v = C_{\eta_1}\sin\theta_1 + C_{\eta_2}\sin\theta_2 \end{cases}. \tag{4.24}$$

Using the expansion $C_j = A_j - iB_j$ for $j = \eta, u, v$, a non-linear system of equations can be derived (6 unknowns). The optimal solution is of the form

$$\cos\frac{\theta_2 - \theta_1}{2} = \pm\frac{A_u B_v - B_u A_v}{\sqrt{\left(A_\eta B_v - B_\eta A_v\right)^2 + \left(B_\eta A_u - A_\eta B_u\right)^2}}, \tag{4.25}$$

which is reintroduced in

$$\left(\cos\frac{\theta_2 + \theta_1}{2}, \sin\frac{\theta_2 + \theta_1}{2}\right) = \frac{\cos\dfrac{\theta_2 - \theta_1}{2}}{A_u B_v - B_u A_v}\left(A_\eta B_v - B_\eta A_v, B_\eta A_u - A_\eta B_u\right), \tag{4.26}$$

to obtain the final solution (θ_1, θ_2).

To conclude, and in both the SDD and DDD methods, the estimated directional spectra follows Schäffer and Hyllested (1994), in which $S(f,\theta)$ was obtained by the convolution of the raw directional spectra with a smoothing window. Extra care needs to be taken as for some frequencies no solution can be found, hence the energy is neglected (5 to 10 % in typical applications). A later study (Hawkes et al., 1997) showed that, for a variety of synthesised sea states that were generated in large wave basins, and despite the fundamental differences between these methods and the stochastic ones, the results were very similar to those obtained with the Maximum Entropy Principle.

4.2.3 Case Study Using Waverider Data

For single-point measuring systems, such as a directional Waverider buoy, valid options are the EMLM, IMLM, EMEP, SDD and DDD methods. Using the recorded displacements in three directions, sensitivity studies relating the major outputs (H_s, dominant direction, etc.) and the evaluation of the corresponding wave roses (polar plots) are valuable to quantify the relative importance of the inputs (like the frequency and directional resolutions, number of iterations, etc.). Figure 4.9 shows the estimated directional spectrum using selected methods for which the computational burden is comparable. Data from a single half-hour file is presented (the sampling frequency of the buoy is equal to 1.28 Hz). The dominant direction is sensitive to the method (oscillating between 280 and 290 compass bearings), but clearly the major differences are between the DFTM method and all

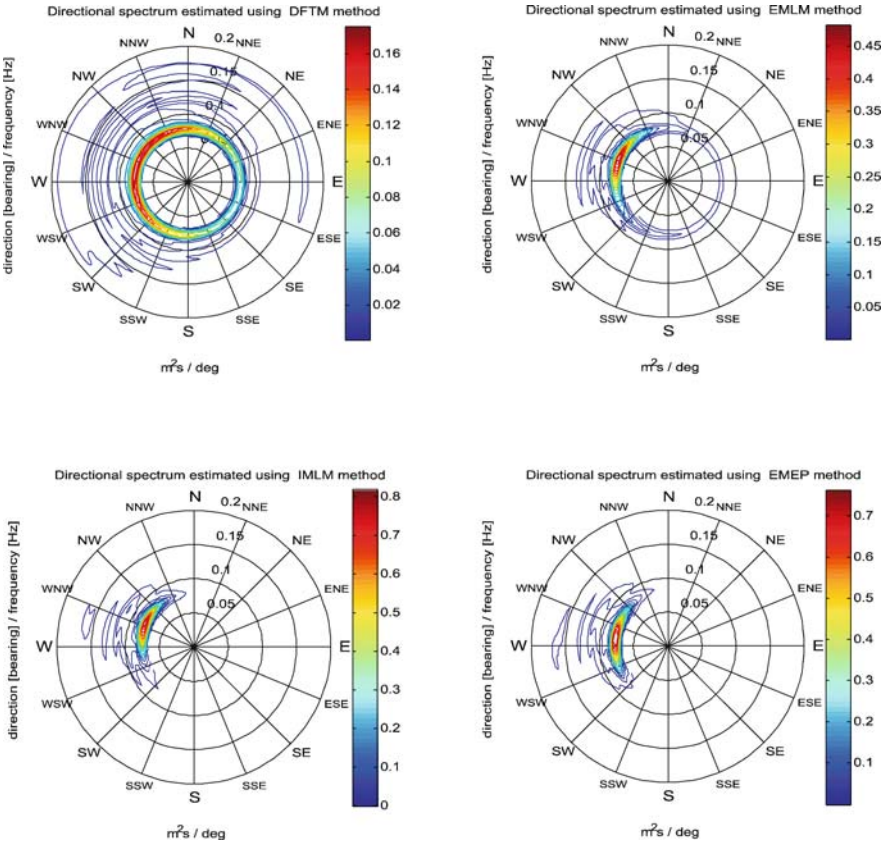

Fig. 4.9. Clockwise (from top left): directional spectrum estimated using the DFTM, ELML, IMLM and EMEP methods (30 *min* of data from a Directional Waverider buoy; $H_{m0} = 4.2\ m$)

the others. The insufficiency of such method in producing a narrow banded spectrum is also clear from Fig. 4.9. The EMLM still produces some fully circular contours (meaning, erroneously, that waves with a certain frequency would come from all directions, with low values of energy density) but greatly minimises the problems of the DFTM algorithm. The low spatial resolution of these methods is also reflected in the differences in the scale of the plots (being broader implies that the maximum values of energy density are naturally reduced). Finally the IMLM and EMEP outputs are similar in shape, though the dominant direction differs by 10 deg (IMLM: 290 compass bearings; EMEP: 280 compass bearings). It is emphasised that certain sea states might be more or less suitable for a specific estimation technique, but as a general rule the latter methods are both more stable and more precise. Several computational packages have been developed to derive the directional spectrum. Johnson (2002) presented the DIWASP toolbox (DIrectional WAve Spectrum) in a MATLAB environment. More recently, Cruz et al. (2007) developed a similar toolbox by emulating other wave analysis packages, applying the methodology to single point measurement systems and implementing a quality check procedure to handle corrupted data sets. Additional estimation methods, such as the wavelet method suggested by Donelan and Krogstad (2005), are to be assessed in futures versions.

4.3 Wave Growth, Travel and Decay

Once created, the sea state is well described as a linear, energy conserving process. However, the generation of waves is a strongly nonlinear process. Energy is input, through air pressure and shear stress, mostly to the high frequency end of the spectrum, and subsequently transferred to lower frequencies through nonlinear wave-wave interactions (Hasselmann 1962, 1963). Also, the waves created are not unidirectional, even in a steady wind, but have a characteristic directionally spread spectrum, centred on the wind direction.

If a steady wind blows over a large expanse of sea, it gradually builds waves up until they reach a state limited by steepness, in which the rate of energy input is balanced by losses through breaking ('white horses'). The limiting state is well described by the simple scaling law formulae of Pierson and Moskowitz (1964)

$$E \propto U^4, \int_0^f S(y)dy = \exp(-k(fU)^{-4}), \tag{4.27}$$

which depend only on the wind speed U. Later empirical work of Mitsuyasu (1975) proposed a formula for the limiting spectrum's directional spread. In this limiting state, the phase velocity is approximately equal to the wind speed, and the steepness (defined by a height to mean wavelength ratio) takes a fixed value. The Froude scale says that the rate of energy input is proportional to U^3 (the usual dependence of wind power on velocity), while the fetch (distance) required for the build-up is proportional to wavelength, and thus to U^2. Therefore the power in a fully developed wind sea is proportional to U^5 (for more detail, see Mollison, 1986).

When the wind speed decreases, waves spread out; their steepness thus decreases, and they cease to lose energy at a significant rate, as long as they remain in deep water. Such waves, separated from the conditions that created them, are known as swell. A typical oceanic sea state may consist of several spectral components: a locally generated wind sea, plus one or more swell components. The latter will typically have narrower spectra as regards both frequency and direction. These various components, to a good approximation, behave in a simple additive fashion, as regards both water movements and energy flows.

4.4 Wave Climate Estimation

Because of its variability on all time scales, a wave climate is not easy to measure. Wave buoys, scalar or directional, can give good estimates of the sea state from a 20 or 30 minute sample, but are too expensive to maintain for long term wave climate estimation, except at a small number of key reference sites. Wave climate estimates have therefore come to rely largely on computer hindcast wind-wave models; for example, the WAM model (WAMDI Group, 1988) now provides global coverage, and has been used, for example, to produce a wave energy atlas (WERATLAS) for European waters (Pontes et al., 1996). Figure 4.10 (from Mollison, 1986) shows estimates of the long-term average resource for Western Europe, made using an earlier wind-wave model. Members of the WERATLAS project team have continued to work over the last decade in the development of what became known as WorldWaves (Barstow et al., 2003). This is an integrated MATLAB package for calculating time series from directional wave spectra and associated statistics anywhere worldwide both in offshore and shallow waters. In a typical project, long term predictions would be made with the models and this would be validated with a few months of in-situ (coastal) buoy measurements. A comparison of synchronous wave model predictions would then allow any model errors to be removed over the longer term.

Normally, data is required for a period of at least 10 years, to allow for seasonal, year-to-year and longer-term variability (such as the El-Nino/Southern Oscillation in the Pacific). For sites in depths of less than $100\,m$, specific consideration of local bathymetry is necessary; and various numerical shallow water models are available that can be used to calculate the nearshore wave climate, starting from data for a deep water reference site (see, e.g., Southgate 1987). For instance, WorldWaves can now provide up to 50-years of wave energy time series at a coastal site, integrating long-term wave model hindcast data with multi-mission satellite altimetry (used for validation and calibration purposes) to specify the incoming deep water waves, long-term buoy data in a few sites, global coastline and bathymetric data and the state-of-the-art SWAN coastal wave model for transferring the offshore climate to the target coastal location.

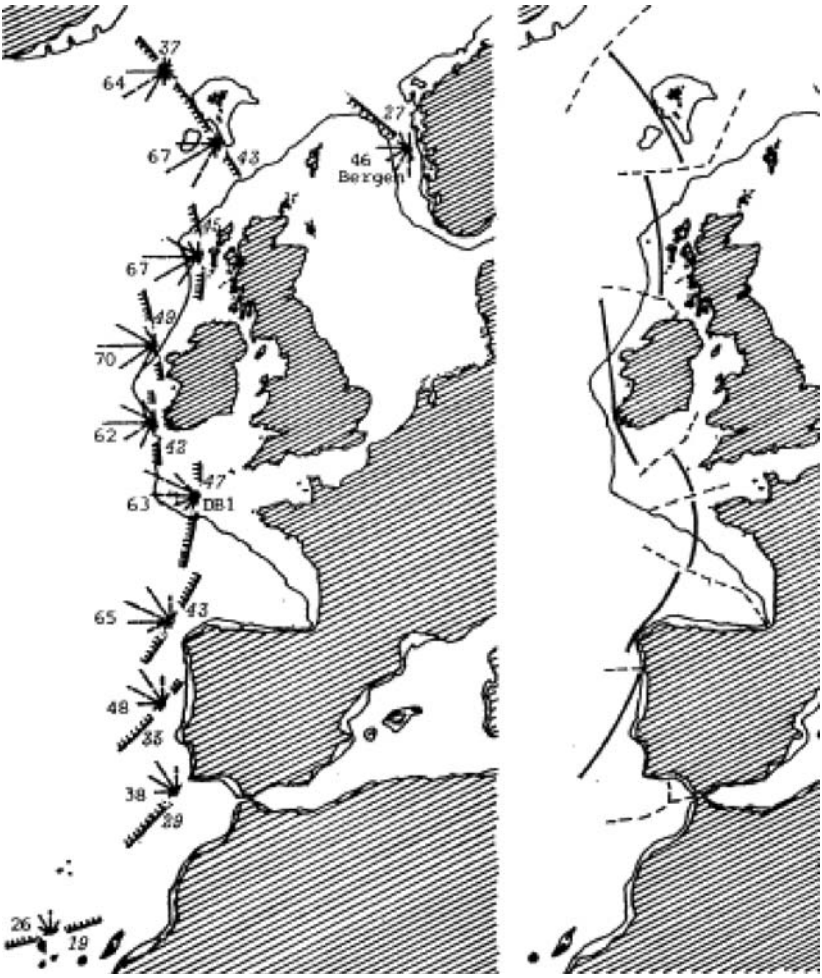

Fig. 4.10. Early wave power estimates for Western Europe (Mollison, 1986)

In the following subsections a review of the main sources of wave data for mapping the wave energy resource is given. Although there are many different types of measurement principle and various types of numerical wave models, only the most relevant for wave energy applications are described. A full review was published recently in Kahma et al. (2005).

4.4.1 Buoys

Buoys have been used for measuring waves since the early 1960s. The most successful has been the Datawell Waverider which measures its own acceleration on a gravity stabilised platform. This sensor was refined in order to also measure the tilt in two orthogonal directions, then allowing for the first time the full directional

spectra. The Hippy 40, as it became known, has been used since the early 1980s. In the mid-1980s, the seminal Wave Direction Calibration Project (WADIC) was carried out at the Ekofisk field in the central North Sea (Allender et al., 1989). All seven of the commercially available wave buoys were compared with regard to a number of platform based wave instrumentation including an array of downlooking laser profilers, current meter triplets, pressure transducers, among other sensors. All but one of the buoys used the Hippy sensor. The OCEANOR Wavescan buoy was particularly successful in WADIC and continues to collect directional wave data today, 23 years after its introduction. It is an example of a so-called heave/pitch/roll buoy. Datawell also paved the way for more reasonably priced directional measurements through its Directional Waverider, launched in the late 1980s. This buoy measures the heave and sway accelerations (outputting the corresponding displacements) rather than the heave, pitch and roll as in the buoys which preceded it. This meant that a more compact spherical hull could be used as measurement platform. Barstow and Kollstad (1991) showed that the Directional Waverider provided reliable data when compared with a Wavescan buoy.

Although the Hippy is still in use, notably in the NOAA network in the USA, most manufacturers of directional buoys have phased it out in preference for more robust sensors without moving parts. Examples are the Seatex Motion Reference Unit (MRU) and the OCEANOR Seasense. The latter is now used in all the buoys shown in Figs. 4.11 and 4.12 (see also Barstow et al., 2005), providing both heave/pitch/roll output for the Wavescan buoy and heave/displacement for the Seawatch buoys.

In offshore waters around the world, long-term buoy wave measurement networks are still relatively few and far between. Networks with directional measurements are even scarcer, even with the clear notion that directional information is essential for a number of applications (e.g.: forecasts, costal defence, etc). Some of the most important networks are:

1. The NOAA-NDBC buoy networks in the US (covering East and West coasts of the USA, the Gulf of Mexico and the Hawaiian Islands), in addition to the more recent Canadian network. Unfortunately, only one of the deep water buoys currently measures directional spectra.
2. The Indian National Data Buoy Programme which is currently probably the largest national program with offshore directional buoys used as standard.
3. National networks in Spain, Greece, France and Italy although most buoys are rather close to the coast and hence quite site specific.
4. Long term measurements carried out in Norwegian waters and the North Sea for the offshore industry.

Fig. 4.11. The Wavescan heave/pitch/roll metocean data buoy has been used for directional wave measurements since 1984 and there are today more buoys than ever in operation, mainly in deep ocean, high current conditions. This buoy has, for example, collected data in the Agulhas current for one year, possibly the toughest environment in the world

Fig. 4.12. The Seawatch buoy (left) and the Seawatch Mini mk. II (right) are used mainly for coastal monitoring. These buoys are examples of heave/displacement buoys. The mini buoy would normally be used for wave energy resource mapping where other metocean parameters such as wind data were not considered to be required

4.4.2 Satellite Altimeters

The back-scattered signal from satellite altimeters, when properly interpreted, can provide significant wave height measurements close to the accuracy of a buoy, from an orbit of typically 1,000 *km* (see, e.g., Krogstad and Barstow, 1999). Measurements are made each second, whilst the satellite flies over a repeat net of ground tracks at about 6 *km/s*. This provides enormous amounts of wave data worldwide, and with, at present, a steady flow of new data from three or more operational satellites, millions of new observations are becoming available each month. Global long-term satellite altimeter measurements have been performed during 1985-1989 by the US Navy's Geosat and the Geosat-Follow-on mission from 2000 by ESA's ERS-1 (from 1991 to 1996), ERS-2 (1996 to 2003), EnviSat (launched in 2002), and most importantly for our purposes due to its longevity, the US/French Topex/Poseidon mission from 1992 to 2005. The Topex-Follow-on mission (Jason) has provided data since 2002. Full resolution altimeter significant wave height and wind speed data for most of these satellites can be found on the World Wave Atlas.

The altimeter is basically a radar which sends a pulse down to the ocean surface at nadir. The significant wave height is obtained from the slope of the leading edge of the return pulse, while the total backscatter gives us the wind speed.

Each satellite altimeter has to be validated and calibrated in order to remove altimeter-dependent biases on significant wave height and this is generally and most reliably done by comparison with long-term offshore buoy data. When comparing temporally varying significant wave height data from the buoy with spatially varying data from the satellite it is important that the buoy measurments are from areas where the gradients in significant wave height are rather small, which means in practice moorings far from coasts as wave conditions often vary rather strongly near to coasts both due to geographical sheltering effects, fetch limited wave growth in offshore blowing winds and shallow water effects.

Emphasis is given here to the Topex satellite altimeter as this is the most successful mission to date. Altimeter data from both the ERS missions as well as Envisat have routinely been assimilated into the ECMWF wave models (see 4.4.3) and are therefore not independent of the model data. Algorithms for the correct interpretation of the back-scattered radar return pulse from satellite altimeters have been gradually improved (see, e.g., Krogstad and Barstow, 1999; Queffeulou, 2004). The accuracy of the Topex altimeter can be seen in the satellite – buoy comparison shown Fig. 4.13. All Topex altimeter data globally for 1992 to 2002 have been analysed applying the bias corrections described above as well as an automatic data control, removing, for example, unphysical along-track variations in wave height. The different satellites fly on different exact repeat orbits, returning to exactly the same ground track on each repeat. The repeat time is 10 days for Topex and Jason, 17 days for Geosat and GFO and 35 days for the ESA satellites. For this reason, the ESA satellites have a much denser coverage spatially, but longer return period to the same location.

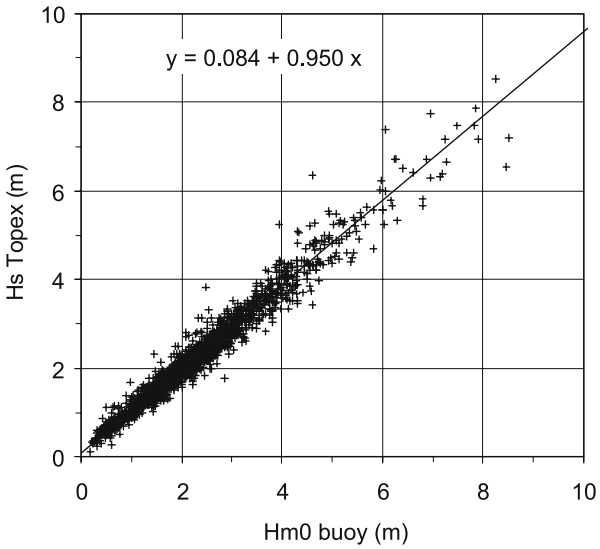

Fig. 4.13. Comparison of significant wave height between the Topex Side B altimeter for 1999–2002 and 13 NOAA buoys; coincident data for Side B. The best fit regression is used to calibrate the satellite wave heights before use

4.4.3 Global Wave Models

Many meteorological centres today run wave models regionally and globally and dedicated long-term hindcasts have also been performed. The wave models simulate the growth, decay and propagation of ocean waves based on input winds over the area in question. In the aforementioned WERATLAS project, it was confirmed that the ECMWF (European Centre for Medium-Range Weather Forecasts) wave model was the best available at that time. ECMWF have maintained that lead (see Fig. 4.14). The reasons for this are related both to the high quality of the ECMWF wind fields and, amongst other things, the assimilation of, in particular, satellite altimeter and also synthetic aperture radar wave data in the models. The WAM wave model (Komen et al., 1994) has been operational at ECMWF since 1992. Further details of the model itself with references can be found at the ECMWF website. The development of the WorldWaves package, through various EU projects, also adopted the ECMWF data.

The current global wave model data base adopted by the WorldWaves project are 0.5º lat/long resolution data from ECMWF's operational global WAM model covering the period December 1996 to present (updated monthly). In addition, for the Mediterranean, Baltic and Black Seas, data are sourced from the finer resolution Mediterranean model. In order to reduce the amount of data, only 1.5 data points are retained in the open ocean areas.

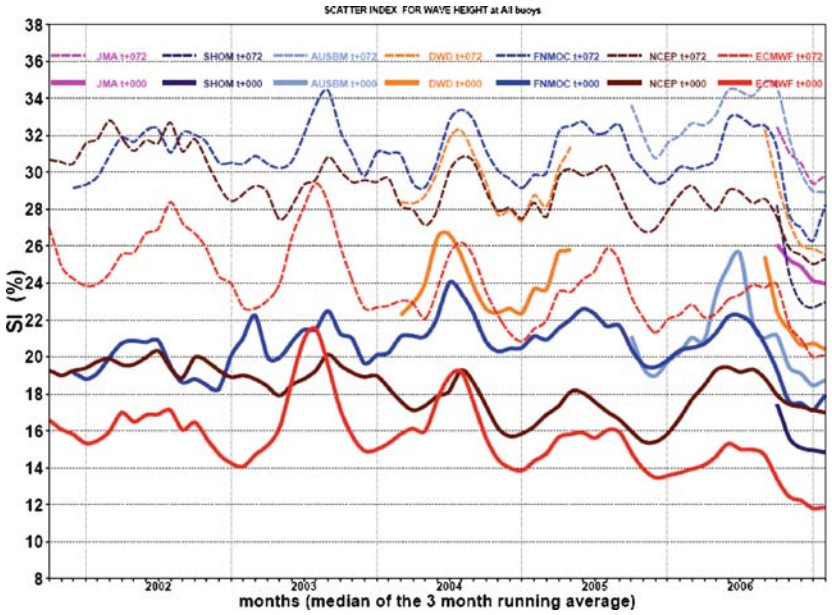

Fig. 4.14. Long-term comparison of the Scatter Index for significant wave height, SI, between model and a multi-buoy data set. The superiority of the ECMWF analysis and forecasts is evident here (the SI is the standard deviation of the difference between the model and buoy normalized by the buoy mean). Figure courtesy of Peter Janssen at ECMWF

In addition, ECMWF have also completed a long-term global ocean wind and wave hindcast (ERA-40 data) which can provide data back to 1957, and, when combined with the operational data up to 50-year time series are available. These data sets are therefore often used in projects requiring longer-term data. The ERA-40 data are, however, run on a coarser 1.5° grid, reducing their usefulness in enclosed sea areas.

The output from the WAM model is the full directional spectrum each 6 hours. When the model data are used as input to a shallow water model (SWAN in WorldWaves), the best results are obtained. These sets are, however, voluminous, and, instead, the wave parameters in Table 4.2 are the default data currently available globally under WorldWaves. Based on the significant wave height, energy period and direction for wind sea and swell separately together with the peak wave period, the full directional wave spectrum is then synthesised when carrying out offshore to nearshore transformations. The full directional spectra files from ECMWF are available from mid-1998 from the operational model at the 0.5º resolution and for the entire ERA-40 hindcast period from mid-1957 to mid-2002 with 1.5º resolution. These data sets are frequently used in projects requiring the highest accuracy.

It is important to understand how the separation of the WAM directional spectra into wind sea and swell parts is carried out. First, the windsea part of the spectrum is defined by

$$1.2\,(28/c)\,U^{*}\cos(\theta-\theta_{w})\geq 1\,, \tag{4.28}$$

Table 4.2 Wave and wind parameters available from the global archives

Parameter long name and units	Alternative short name
Significant wave height, *m*	H_{m0} or H_s
Mean wave direction, *deg*	
Peak period of 1d spectra, *s*	T_p
Energy period, *s*	T_{m-10}, T_{-10} or T_e
Significant wave height for the wind waves, *m*	$H_{m0\,ws}$ or $H_{m0\,w}$
Mean direction of wind waves, *deg*	M_{dirws}
Mean period of wind waves, *s*	$T_{m-10\,ws}$ or $T_{m-10\,w}$
Significant wave height for the swell, *m*	$H_{m0\,sw}$ or $H_{m0\,s}$
Mean direction for the swell, *deg*	M_{dirsw}
Mean period for the swell, *s*	$T_{m-10\,sw}$ or $T_{m-10\,s}$
Wind speed equivalent to 10 *m* height, 10 *min*. average, *m/s*	W_{sp} or U_{10}
Wind direction Eq. to 10 *m* height, 10 *min*. average, *deg*	θ_w

where $c = c(f)$ is the phase speed of the waves with frequency f and U^* is the friction velocity. If τ is the surface stress then

$$\tau = U^{*2} = C_d U_{10}^2, \tag{4.29}$$

where C_d is the drag coefficient and U_{10} is the 10 *m* wind speed. θ is the mean propagation direction of the waves and θ_w is the direction of the wind. What is not wind sea is then classified as swell.

In some parts of the world (e.g., the Pacific coasts of South America), two or more swells can frequently coexist. In this case, the three parameters describing the swell spectrum will poorly describe the swell energy-direction spectrum. In such areas, the full directional spectra data must then be used when trying to predict coastal wave conditions. At any offshore location in the Pacific in the northern winter (October to March), crossing northerly and southerly swells will frequently occur. Using parameter data for predicting coastal wave energy resources will for this reason either over- or under-predict, often significantly, even if the models were perfect.

4.4.4 Model Validation and Calibration

The satellite altimeter data represent a high quality, independent and globally covering wave and wind data set which can be used for the direct validation of wave model data, even though this is limited to significant wave height and wind speed. The correlation between satellite and buoy data were confirmed using long-term data sets from the NOAA wave buoy network. The WAM model significant wave heights are compared first against 13 NOAA buoys and then against satellite altimeter data sampled from the area around each of the same buoys. From the resultant scatter plots for each of the 13 locations, various statistics were calculated. The results in the form of the bias and the scatter index are presented in the maps in Figs. 4.15 and 4.16. As it can be seen, the results are more or less identical independent of whether one chooses the buoy or satellite data for the validation. This gives us the confidence to use the Topex data globally as a reliable reference, as if a worldwide buoy network was available.

The wave model data is available on a regular 0.5º lat-long grid. The satellite data are, on the other hand, available about each 6 *km* each *N*-days (where *N* is the exact repeat period for each satellite) along ground tracks globally. In the World-Waves project, a global offshore wave model data set was created using the corrected (against buoy data) Topex data from 1996 to 2002 to validate and subsequently calibrate the ECMWF model data. This was found to be worthwhile as there was typically a systematic bias on the raw model data. Removing that bias significantly improves the data quality, particularly in enclosed seas such as the Mediterranean. Not all grid points are close enough to a Topex satellite track to be useful for validation purposes (i.e., considered to be derived from the same wave climate population). Thus, a sub-set of calibration points were identified. Of a total of about 10,000 wave model grid points globally about 5,700 are calibration points (in oceanic areas, practically all points are validation points as there are not strong wave climate gradients in such areas) and a larger spatial separation between model and satellite data for calibration is acceptable. Near coastal waters, the selection of calibration points and satellite data extraction locations used for validation has to be done manually as it is not necessarily the closest point which is the best choice in such areas with strong wave gradients.

The results of the global model validation are presented in Fig. 4.17 (correlation coefficient). Although showing a largely very high correlation, the model tends to underestimate the significant wave height in a systematic way. Using the regression coefficients to calibrate the model data removes the bias and gives more accurate offshore boundary conditions for coastal wave modelling. Since 2002, significant improvements have been made to the ECMWF models and the bias is now much reduced. The global validation is currently being repeated using the Jason altimeter data (this satellite flew the same ground tracks as Topex and the same validation points can therefore be used). The validation can be further refined by using data from all satellite altimeter missions. This is particularly advantageous in areas with relatively strong wave climate gradients.

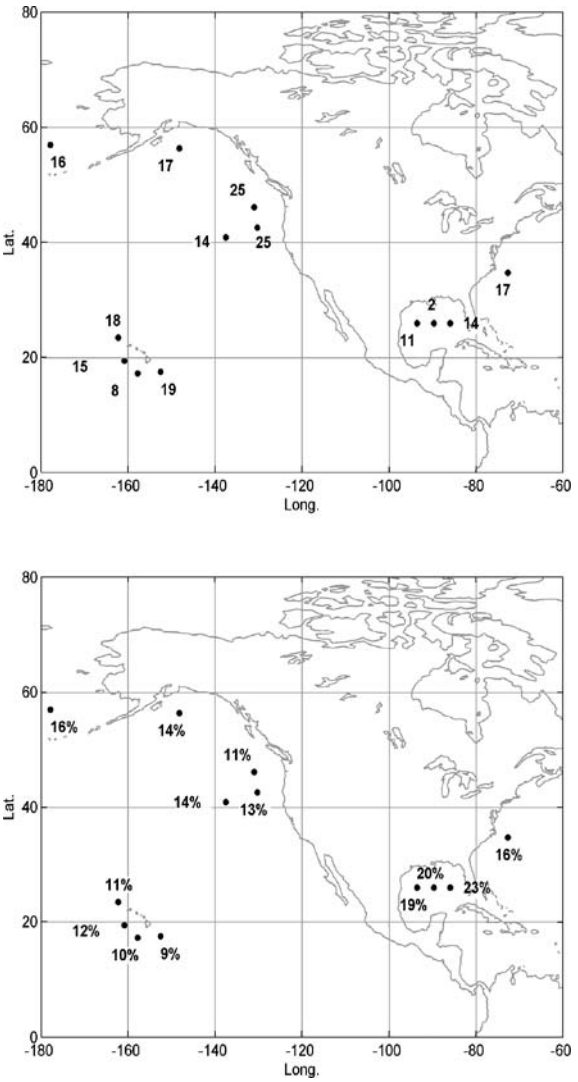

Fig. 4.15. Validation statistics of H_{m0} from WAM against NOAA buoy data for 1996 to 2002. Top: mean difference in *cm*; Bottom: residual Scatter Index in %

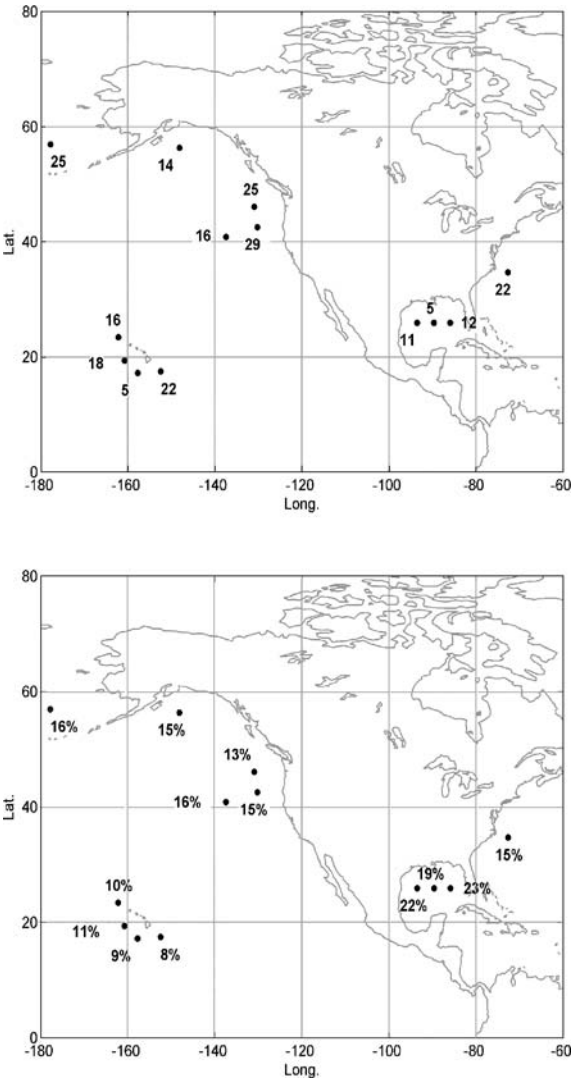

Fig. 4.16. Validation statistics of H_{m0} from WAM against calibrated Topex data for the locations of the NOAA buoys in Fig. 4.16 for 1996 to 2002. Top: mean difference in cm; Bottom: residual Scatter Index in %

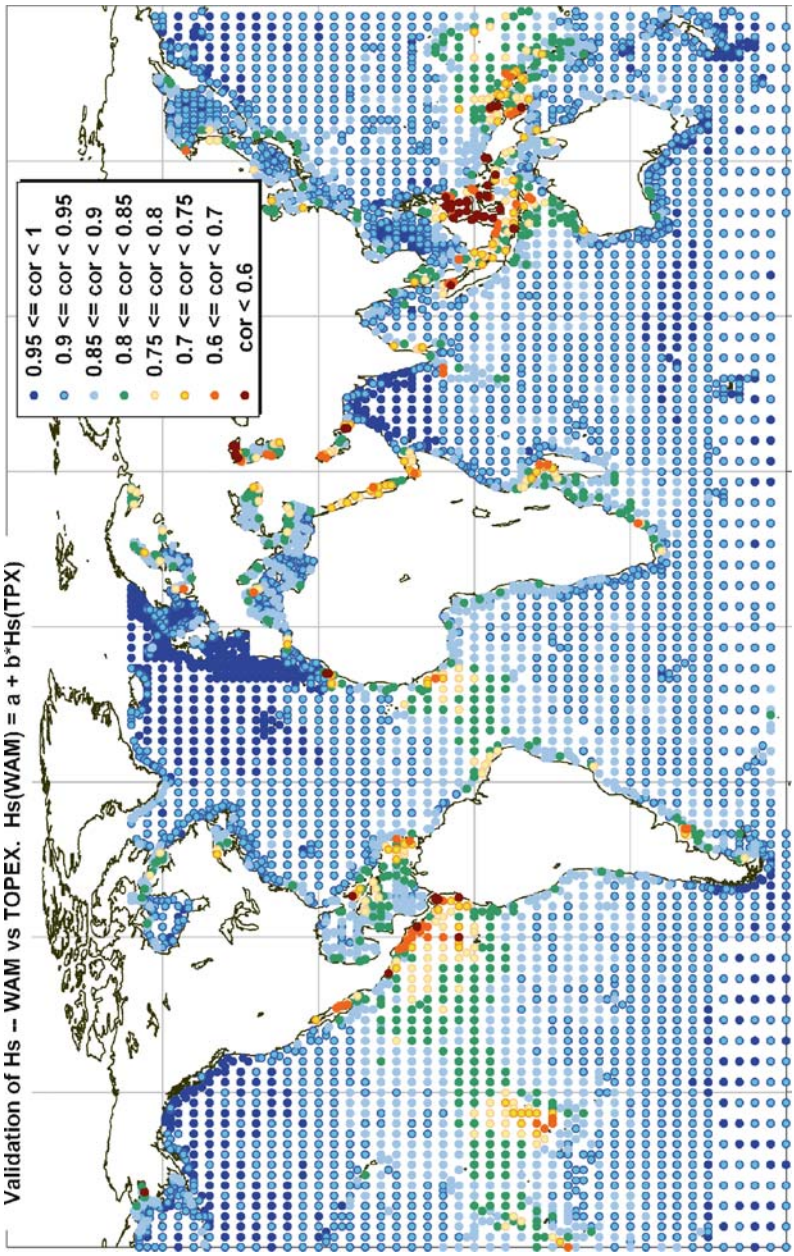

Fig. 4.17. Global map showing the correlation coefficient between the ECMWF WAM operational model data and Topex/Poseidon data for all global validation points for December 1996 to 2002

The ECMWF model was then finally calibrated on a global basis for inclusion in the WorldWaves software package. This was done by adjusting significant wave heights and, analogously, the wind speed on a point-by-point basis for all global grid points. For oceanic points, wave periods were adjusted to conserve the wave steepness in some enclosed seas where wind sea dominates. Directional wave spectra can also be calibrated on a case-by-case basis.

Such an approach, combining an 'Atlas' data base for offshore reference sites with computer tools for calculating the resource at specific locations, was pioneered for the evaluation of the UK wave energy resource by Whittaker et al. (1992). This two-level methodological approach has major advantages of flexibility and long life, in that the components – both data base and computer tools – can be updated individually as relative technological advances are made.

4.5 Wave Energy in Shallow Water

Once waves enter shallow water, roughly defined as water of depth less than half a wavelength, they change in a number of respects. For a start, the basic solutions of the equations for surface waves under gravity are different, because of the lower fixed boundary to water movement. In the extreme, where the wavelength is much greater than the water depth, the group velocity is no longer half the phase velocity but equal to it. This means that waves are no longer dispersive, but travel as solutions: the classic example of this is a tsunami, where waves with a wavelength of 100 km or more can be created by a sudden fall or rise in the sea floor. On a much more modest scale, the same behaviour can be seen when an ocean swell runs up a gently sloping beach. As ocean waves enter shallow water, they slow down; for a wave approaching at an angle to the depth contours this has the effect of changing its direction; the wave spectrum consequently becomes narrower directionally, with principal direction close to perpendicular to the depth contours.

In slowing down, the wavelength decreases and height increases, leading to breaking. Waves lose energy both through breaking and through bottom friction, which can be significant in depths from 50 m to around 100 m (Mollison, 1983).

In WorldWaves, the offshore model data sets described in section 4.4 are used as boundary conditions to the state-of-the-art SWAN model (Booij et al., 1999) for calculating coastal wave conditions anywhere worldwide. SWAN then performs the offshore to nearshore transformation for each time step, generating a new time series of wave parameters and/or full directional spectra at the nearshore target location(s) of interest. Geographic tools are available for quickly selecting any geographical area worldwide for the analysis, setting up a computational area with nesting and selecting the offshore boundary grid points and target nearshore locations.

SWAN is a third-generation spectral wave model, developed for the calculation of the propagation of random waves from deep to shallow water, accounting for the following physics:

- Wave propagation in time and space, including the effects of shoaling, refraction due to current and depth, frequency shifting due to currents and the effects of non-stationary depth;
- Wave generation by wind;
- Triad and quadruplet non-linear wave-wave interactions;
- Whitecapping, bottom friction, and depth-induced breaking;
- Wave induced setup;
- Transmission through and reflection from obstacles.
- Wave diffraction

A typical project will involve the following stages:

- Select and recalibrate the offshore model points using validation data from all satellite altimeters providing data near to the grid points to be used in the offshore to nearshore transformation. Calibrate the full offshore directional spectra.
- Check and update the bathymetric data from admiralty charts.
- Set up the computational grid with suitable choices of grid meshes (both in the outer and nested grids) and other relevant SWAN parameters controlling model physics and numerics.
- Run SWAN for the time period of interest, taking account of water level variations in shallow target locations where tides and storm surge can significantly impact the resource and design conditions.
- Quality control the nearshore time series data.
- Calculate the required wave statistics.

In some cases, one might have satellite data near to the target location which could be used to check the offshore to nearshore transformation. If not, it is wise to carry out short term buoy measurements at the target location to validate the model results (note that the SWAN simulation can be updated for exactly the same time period as the measurements to give the possibility of direct validation). If bias is found between the SWAN simulations and the measurements, this information can be used, for example, to calibrate the long-term model predictions.

As waves move from deep water into shallower water, the ratio of maximum to mean wave energy can decrease considerably. In a simulation where the wave transformation across the shelf and towards the coast of Southern Australia was modelled using the SWAN wave model the maximum storm wave energy is reduced relative to the mean by about a factor of 3 from 50 to 6 m water depth. It also became clear that the extremes are reduced by a much large amount than the normal (average) sea states.

4.6 Discussion

In this chapter a detailed account of the origin and methods to estimate the wave energy resource were given. Resource assessment studies are essential when evaluating the possible locations for a wave energy project, and site specific measurements and surveys are necessary prior to any final decision on where to install a wave farm. As demonstrated, for a first selection of suitable areas numerical models play an important role and their validation is critical.

In an operational environment, the understanding of the incoming wave field and its correlation with the performance of the wave energy converter(s) is crucial, hence the emphasis given to the several methods to estimate the directional spectrum. Wave measurement systems that are capable of delivering such information, such as surface buoys or bottom-mounted acoustic Doppler current profilers (ADCPs), are commercially available but it is likely that a new wave energy industry will have additional specifications for such devices like, e.g., increased sampling frequency, longer autonomy, etc.

This contribution aims to show to the readers the areas in the globe where wave energy projects are more likely to be installed and to present the considerable amount of experience that can be emulated from the offshore industry and from oceanography. Those interested in extending their knowledge in this field can find suitable references in the articles mentioned throughout the chapter and in key textbooks such as Goda (2000) and Tucker and Pitt (2001). A vital area (forecasting) should also be approached by such readers, as it strongly affects the O&M aspects of a wave energy farm.

References

Akaike H (1973) Information theory and an extension of the maximum likelihood principle. In: Petrov, Csaki (eds) Proc 2nd Int Symp Inform Theory. Akademiai Kiado, Budapest, pp 267–281

Allender J, Audunson T, Barstow S, Bjerken S, Krogstad HE, Steinbakke P, Vartdal L, Borgman L, Graham C (1989) The WADIC Project: A comprehensive field evaluation of directional wave instrumentation. Ocean Eng 161:505–536

Barber NF (1961) The directional resolving power of an array of wave detectors. Ocean Wave Spectra. Prentice-Hall, pp 137–150

Barstow SF, Aasen SE, Mathisen JP (2005) WaveSense marks the first 20-years service for the Wavescan buoy. Sea Technol, pp 53–57

Barstow SF, Kollstad T (1991) Field trials of the Directional Waverider. In: Proc 1st Int Off Pol Eng Conf (ISOPE), pp 55–63

Barstow SF, Mørk G, Lønseth L, Schjølberg P, Machado U, Athanassoulis G, Belibassakis K, Gerostathis T, Stefanakos CN, Spaan G (2003) WorldWaves: Fusion of data from many sources in a user-friendly software package for timely calculation of wave statistics in global coastal waters. Proc 13th ISOPE Conf. Oahu, Hawaii, USA

Benoit M (1992) Practical comparative performance survey of methods used for estimating directional wave spectra from heave-pitch-roll data. In: Proc 23rd Int Conf Coastal Eng (ASCE). Venice, Italy, pp 62–75

Benoit M, Frigaard P, Schäffer HA (1997) Analysing Multidirectional Wave Spectra: A Tentative Classification of Available Methods. In: Proc IAHR Sem Multidirectional Waves Interact Struct. 27th IAHR Congress. San Francisco, USA, pp 131–158

Booij N, Ris RC, Holthuijsen LH (1999) A third-generation wave model for coastal regions. 1. Model description and validation. J Geophys Res 104(C4):7649–7666

Capon J, Greenfield RJ, Kolker RJ (1967) Multidimensional maximum-likelihood processing of a large aperture seismic array. Proc IEEE 55:92–211

Cruz J, Mackay E, Martins T (2007) Advances in Wave Resource Estimation: Measurements and Data Processing. Proc 7th Eur Wave Tidal Energy Conf. Porto, Portugal

Donelan M, Krogstad H (2005) The Wavelet Directional Method. In: Khama et al. (eds) Measuring and analysing the directional spectra of ocean waves. EU Cost Action 714.71–80

Goda Y (2000) Random seas and design of maritime structures, 2nd edn. World Scientific Publishing

Hagerman G (1985) Oceanographic design criteria and site selection for ocean wave energy conversion. In: Proc IUTAM Sym Lisbon 1985. Hydrodynamics of Ocean Wave Energy Utilization. Springer Verlag

Hashimoto N, Kobune K, Kameyama Y (1987) Estimation of directional spectrum using the Bayesian approach and its application to field data analysis. Rep Port Harbour Res Inst, Vol. 26

Hashimoto N, Nagai T, Asai T (1994) Extension of Maximum Entropy Principle for directional wave spectrum estimation. In: Proc 24th Int Conf Coastal Eng (ASCE). Kobe, Japan, pp 232–246

Hasselmann K (1962) On the nonlinear energy transfer in a gravity-wave spectrum. 1. General theory. J Fluid Mech 12:481–500

Hasselmann K (1963) On the nonlinear energy transfer in a gravity-wave spectrum. 2. Conservation laws, wave-particle correspondence, irreversibility. J Fluid Mech 15:273–281

Hawkes PJ, Ewing JA, Harford CM, Klopman G, Stansberg CT, Benoit M, Briggs MJ, Frigaard P, Hiraishi T, Miles M, Santas J, Schäffer HA (1997) Comparative Analyses of Multidirectional Wave Basin Data. In: Proc IAHR Sem Multidirectional Waves Interact Struct, 27th IAHR Congress. San Francisco, USA, pp 25–88

Isobe M, Kondo K, Horikawa K (1984) Extension of MLM for estimating directional wave spectrum. In: Proc Symp Descript Model Directional Seas, Paper A-6. Lingby, Denmark

Isobe M (1990) Estimation of directional spectrum expressed in a standard form. In: Proc 22nd Int Conf Coastal Eng (ASCE), pp 467–483

Johnson D (2002) DIWASP, a directional wave spectra toolbox for MATLAB: User Manual. Research Report WP-1601-DJ (V1.1). Centre for Water Research, University of Western Australia

Kahma K, Hauser D, Krogstad HE, Lehner S, Monbaliu JAJ, Wyatt L (2005) Measuring and Analysing the Directional Spectra of Ocean Waves. EU COST Action 714. EUR 21367. ISBN 92-898-0003-8

Kinsman B (1965) Wind Waves. Prentice-Hall, pp 460–471

Komen GJ, Cavaleri L, Donelan M, Hasselmann K, Hasselmann S, Janssen PAEM (1994) Dynamics and Modelling of Ocean Waves. Cambridge Univ Press

Krogstad HE, Barstow SF (1999) Satellite Wave Measurements for Coastal Engineering Applications. Coastal Eng 37:283–307

Kuik AJ, van Vledder G, Holthuijsen LH (1988) A Method for the Routine Analysis of Pitch-and-Roll Buoy Wave Data. J Phys Oceanogr 18:1020–1034

Longuet-Higgins MS, Cartwright DE, Smith ND (1963) A variational technique for extracting directional spectra from multicomponent wave data. J Phys Oceanogr 10:944–952

Longuet-Higgins MS (1985) Accelerations in steep gravity waves. J Phys Oceanogr 15:1570–1579

Lygre A, Krogstad H (1986) Maximum Entropy Estimation of the Directional Distribution in Ocean Wave Spectra. J Phys Oceanogr 16:2052–2060

Mitsuyasu H, Tasai, F, Suhara T, Mizuno S, Ohkuso M, Honda T, Rikishi K (1975) Observations of the directional spectrum of ocean waves using a cloverleaf buoy. J Phys Oceanogr 5:750–760

Mollison D (1983) Wave energy losses in intermediate depths. Appl Ocean Res 5:234–237

Mollison D (1986) Wave climate and the wave power resource. In: Evans DV, Falcao Af de O (eds) Hydrodynamics of Ocean Wave–Energy Utilization. Springer–Verlag, Heidelberg, pp 133–156

Mollison D (1994) Assessing the wave energy resource. In: Barnett V, Turkmann KF (eds) Statistics for the Environment 2: Water Related Issues. Wiley, pp 205–221

Pawka SS (1983) Island shadows in wave directional spectra. J Geophys Res 88(C4):2579–2591

Pierson WJ, Moskowitz L (1964) A proposed spectral form for fully developed wind seas based on the similarity theory of SA Kitaigorodskii. J Geophys Res 69:5181–5190

Pontes MT et al. (1996) An atlas of the wave-energy resource in Europe. J Offshore Mech Arctic Eng 118:307–309

Queffeulou P (2004) Long term validation of wave height measurements from altimeters. Marine Geod 27:495–510

Sand SE (1984) Deterministic Decomposition of Pitch-and-Roll Buoy Measurements. Costal Eng 8:242–263

Schäffer HA, Hyllested P (1994) Analysis of Multidirectional Waves Using Deterministic Decomposition. In: Proc Int Symp: Waves – Physical and Numerical Modelling. Univ British Columbia, Vancouver, Canada, pp 911–920

Southgate HN (1987) Wave prediction in deep water and at the coastline. Report SR 114. HR Wallingford, UK

Tucker MJ, Pitt EG (2001) Waves in Ocean Eng. Elsevier Science Ltd, London

WAMDI Group (1988) The WAM Model – a third-generation ocean wave prediction model. J Phys Oceanogr 18:1775–1810

Whittaker TJT et al. (1992) The UK's Shoreline and Nearshore Wave Energy Resource. UK Dept of Trade & Industry, ETSU WV 1683

Woolf DK, Cotton PD, Challenor PG (2003) Measurement of the offshore wave cli mate around the British Isles by Satellite Altimeter. Philos Trans R Soc Lond Ser A, pp 27–31